Biochimica et Biophysica Acta, 436 (1976) 260–282

BBA 77339

LIGHT SCATTERING AND TURBIDITY MEASUREMENTS ON LIPID VESICLES

C. S. CHONG and KONRAD COLBOW

Department of Physics, Simon Fraser University Burnaby, B.C. V5A 1S6 (Canada)

(Received February 3rd, 1976)

SUMMARY

The dynamic behaviour of model membranes in the form of sonicated liposomes in excess water was studied by means of 90 °C light scattering and turbidity measurements. Computer calculations based on the Rayleigh-Gans theory of light scattering were used to estimate the average size of lipid vesicles dispersed in water, taking into account the various structures of the vesicles. Normal reversible changes in the scattered light intensity and turbidity with temperature could be accounted for mainly by the change in the refractive index of the lipid and irreversible anomalous changes were explained on the basis of fusion of smaller aggregated vesicles.

INTRODUCTION

In 1881 Lord Rayleigh published his theoretical work [1] on scattering by particles much smaller than the wavelength of the scattered light. This is usually referred to as Rayleigh scattering. Approximate theory for particles with dimensions comparable to the wavelength of the incident radiation was developed later by Rayleigh [2], Debye [3], and Gans [4]. This type of scattering is called Rayleigh-Gans scattering or Rayleigh-Debye scattering. The problem was solved in a rigorous fashion for spheres of arbitrary size by Mie [5] and independently by Debye [6] and is commonly referred to as the Mie theory. The reader is referred to excellent books on light scattering by Van de Hulst [7] and by Kerker [8].

Light scattering methods have often been used to determine sizes and shapes of cells, subcellular particles and phospholipids dispersed in water. Koch [9] employed the Rayleigh-Gans approximation to estimate the size of mitochondria and of *Escherichia coli* bacteria. Physiocochemical differences between fragments of plasma membrane and endoplasmic reticulum were studied by Wallach et al. [10] using turbidity measurements. Atwood and Saunders [11] studied by light scattering changes in the size and shape of egg lecithin aggregates sonicated for varying lengths of time.

Thermotropic phase transitions in both natural and model membranes dispersed in water have also been observed by light scattering and turbidity methods. Abramson [12] observed a decrease in turbidity of an aqueous dispersion of dipalmi-

toyllecithin in the range from 24 to 33 °C and a sharp decrease at the transition temperature of 41 °C. A sharp decrease in scattered light intensity at the phase transition was also observed for isolated phospholipids, and membranes of the fatty acid auxotroph of *E. coli* supplemented with different fatty acids in the growth medium [13, 14].

Theoretical studies on the scattering of phospholipid dispersions have been made on the assumption of a spherical shell model for the lipid vesicle [15, 16]. Such a model is applicable to microvesicles prepared by the method of Huang [17]. However, for normal preparations of phospholipid dispersions, electron micrographs often reveal onion-shaped multilamellar liposomes of various sizes [18, 19]. Also aggregates of lyposomes were often observed. The size of vesicles also has an effect on their NMR spectral characteristics. Large vesicles with multilamellar structure showed broad resonances whereas smaller vesicles showed sharp resonances [20, 21].

The sizes and shapes of vesicles observed in electron micrographs often depend on the fixing or staining method used. Light scattering offers the distinct advantage that the system can be observed without significant perturbations. A standard spectrometer is often easily adapted to measure light scattering. One may either observe the scattered light at right angle to the incident beam or measure the turbidity. The latter is the decrease by scattering of the transmitted light, and thus is equal to the scattering over all angles. The interpretation of the scattering data has often been

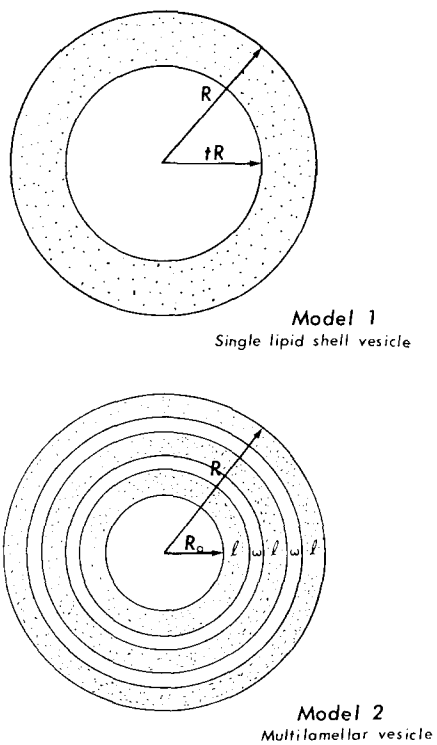

Fig. 1. Models of lipid vesicle structure.

difficult in the past. However, recent progress [22] has enabled us to use scattering information to characterise membrane vesicle size and distribution, and to distinguish between single-walled and onion-shaped multilamellar liposomes varying in size from a few micrometers down to a fraction of 1 μm [22].

This paper deals with light scattering and turbidity measurements of dipalmitoyl-lecithin dispersions, prepared by sonication for different lengths of time, followed by filtration with metricel filters or ultracentrifugation. A measurement of the turbidity of the dispersion as a function of wavelength using a spectrophotometer provides a means of evaluating the average size and structure of the vesicles in the dispersion. For this purpose, we have made computer calculations based on the Rayleigh-Gans theory of light scattering for two models of the lipid vesicles (see Fig. 1). We have calculated the scattering parameters as a function of particle size for a system of particles of uniform size (monodispersed) as well as for a polydispersed system with a log-normal size distribution. We illustrate the application of the calculations with several lipid dispersions prepared in a variety of ways. We also used light scattering and turbidity measurements to study the lipid phase transition, liposome aggregation and fusion.

EXPERIMENTAL

Synthetic DL-α-lecithin (also known as β,γ-dipalmitoyl-DL-α-phosphatidylcholine) was purchased from Sigma Chemical Co. Thin-layer chromatography showed only one spot and the lipid was used without further purification.

Dispersions were prepared by sonicating the lipid in doubly distilled water using the Biosonik IV ultrasonic apparatus with a titanium probe operated at fixed power for varying lengths of time. No buffer was used and the pH values of the dispersions were within 6.3 ± 0.2. During sonication, the samples were immersed in a cold water (16 °C) circulation bath. The dispersions were then divided into portions for filtration with 1.0 or 0.2 μm pore Gelman metricel filters or for centrifugation at $20\,000 \times g$ for 0.5 h. Known volumes of the final portions were used to estimate the lipid content by the colorimetric method of Raheja et al. [23]. The initial concentrations of the dispersions were usually about 1 mg/ml. The experimental arrangement for light scattering is shown in Fig. 2. The light source was a high pressure 100 W mercury lamp (PEK Lab. type 112) and the wavelength of the incident light was selected to be 436 nm using a Jarell-Ash 1/4 meter Ebert monochromator with 1 mm slits. The scattered light was focussed onto a second Jarell-Ash monochromator set at the same wavelength and detected by an EMI 9558 photomultiplier (S-20 response). Part of the incident light was reflected off by a quartz slide to a RCA 935 phototube. Signals from both detectors were amplified by phase-lock amplifiers and then fed into a Philbrick Q3-MIP divider. The output from the divider was displayed on a chart recorder. This procedure eliminated error due to variation in lamp intensity. The lens behind the excitation monochromator was adjusted to give a collimated parallel incident beam. A diaphragm was placed in the path of the scattered beam to limit the aperture to less than 5° half angle. Vertically polarized incident light was used throughout and normally only the vertical component of the scattered light was measured as a function of temperature. The vesicle dispersion was placed in a 1 cm^2 quartz cell placed tightly into a specially milled brass block through which water could circulate.

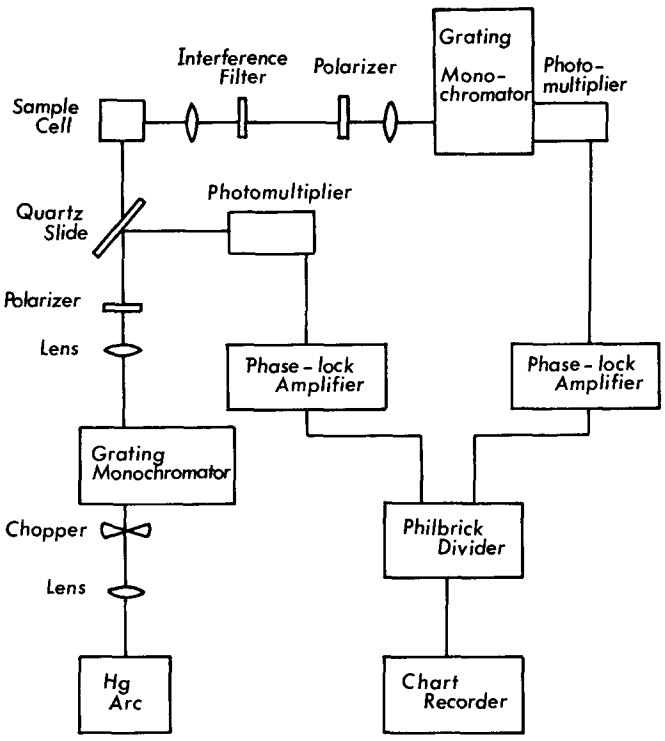

Fig. 2. Experimental set-up for light scattering measurements.

Temperature control was obtained with a Haake FT thermostated circulation pump. The temperature was varied at the rate of 1 °C per min and usually two heating-cooling cycles were run for each sample.

Turbidity was measured using a Cary-14 spectrophotometer equipped with thermostatic control for 1 cm^2 cuvets; the wavelength scan extended from 300 to 650 nm.

The refractive index was measured with a Bausch and Lomb 3L refractometer, which gave direct measurements for the sodium-D line (589 nm). To obtain the refractive index variation with concentration a set of dispersions with lipid concentrations of 1–10 % was used. The dependence of refractive index on wavelength was estimated using tables supplied by the manufacturer. All samples were mildly sonicated and measurements on four sets of samples were taken. Temperature dependence of the refractive index was measured on a dispersion of 10 % lipid concentration.

THEORY OF LIGHT SCATTERING

In the Rayleigh-Gans theory of light scattering [2, 4], the intensity scattered per unit volume of solution by N isotropic particles per unit volume is [22]

$$\frac{I(\theta)}{I_0} = \frac{N}{2}\left(\frac{3\pi V}{r}\right)^2\left(\frac{n}{\lambda}\right)^4\left(\frac{m^2-1}{m^2+2}\right)^4(1+\cos^2\theta)P(\theta) \qquad (1)$$

$m = n_0/n$ is the relative refractive index, where n_0 is the refractive index of the particle and n that of the medium. I_0 is the incident intensity, V the volume of material in a particle, r the observation distance, λ the incident wavelength in vacuum and θ is the angle of observation measured from the incident beam. The scattering factor $P(\theta)$ is a correction factor to normal Rayleigh scattering and accounts for the interference of light scattered from different parts of the particle. $P(\theta) \to 1$ for particles much smaller than λ.

Integrating over the surface of a sphere of radius r yields the total light scattered

$$S = 24\pi^3 V^2 N \left(\frac{n}{\lambda}\right)^4 \left(\frac{m^2-1}{m^2+2}\right)^2 I_0 Q \tag{2}$$

Q is called the dissipation factor:

$$Q = \frac{3}{8}\int_0^{\pi} \mathrm{P}(\theta)(1+\cos^2\theta)\sin\theta \mathrm{d}\theta \tag{3}$$

Similar to Beer-Lambert's law for absorption, the transmitted light intensity I is written as

$$I = I_0 \exp(-\tau d) \text{ or } I = I_1 10^{-Ad}, \tag{4}$$

where the attenuation constant τ is called the turbidity, d is the path-length and A the absorbance of the sample is the quantity measured with the spectrophotometer. It is readily seen that

$$\tau = 2.303A = 24\pi^3 V^2 N \left(\frac{n}{\lambda}\right)^4 \left(\frac{m^2-1}{m^2+2}\right)^2 \tag{5}$$

Rayleigh [2], and Gans [4] considered the interference of light scattered from different parts of the particle but neglected the phase changes in light traversing the particle. This assumes that the refractive index of the particle is close to that of the medium, and that $4\pi nR(m-1)/\lambda \ll 1$. The scattering factor $P(\theta)$ for spherically symmetric particles with continuous scattering elements, is given by the square of the form factor [8]

$$f = \frac{\int_0^{\infty} 4\pi r^2 G(r) \dfrac{\sin kr}{kr} \mathrm{d}r}{\int_0^{\infty} 4\pi r^2 G(r) \mathrm{d}r} \tag{6}$$

where $k = (4\pi n/\lambda)\sin(\theta/2)$ and $G(r)$ is the radial distribution function. $P(\theta)$ can be written in simple analytic form for some common particle shapes. For a shell of thickness $(1-t)R$ [24]

$$P(\theta) = \left[\frac{3}{(1-t^3)Z^3}(\sin Z - Z\cos Z + tZ\cos Z - \sin tZ)\right]^2 \tag{7}$$

where $Z = kR$.

For a multilammelar structure of y concentric lipid shells each of thickness l enclosing water of thickness ω between the shells (Fig. 1) we find [22]

$$P(\theta) = \left\{\frac{4\pi}{k^3 V}\sum_{j=1}^{y}[\sin kx_j - \sin k(x_j-l) + k(x_j-l)\cos k(x_j-l) - kx_j \cos kx_j]\right\}^2 \quad (8)^\star$$

where $x_j = R_0 + (j-l)\omega + jl$, and R_0 is the radius of the central water core. V is the total volume of lecithin material in the structure and is given by

$$V = \frac{4\pi}{3}\sum_{j=1}^{y}[x_j^3 - (x_j-l)^3] \quad (9)$$

To express $I(\theta)$ and τ in terms of more directly measurable parameters, we note that

$$n(m-1) = (M/V)(\mathrm{d}n/\mathrm{d}c) \quad (10)$$

where M is the anhydrous mass of a single particle, c the concentration of dipalmitoyl-α-phosphatidylcholine and $\mathrm{d}n/\mathrm{d}c$ is the measured refractive index increment. Thus, with $c = MN$, we finally get the expressions for the specific intensity and the specific turbidity

$$\frac{I(\theta)}{c} = \frac{9}{2}\frac{\pi^2 n^3 V}{r^2\lambda^4}\frac{\mathrm{d}n}{\mathrm{d}c}\frac{(m+1)^2(m-1)}{(m^2+2)^2}(1+\cos^2\theta)P(\theta)I_0, \quad (11)$$

$$\frac{\tau}{c} = 24\frac{\pi^3 n^3 V}{\lambda^4}\frac{\mathrm{d}n}{\mathrm{d}c}\frac{(m+1)^2(m-1)}{(m^2+2)^2}Q \quad (12)$$

From Eqn. 12 we obtain the derivative

$$-\frac{\mathrm{d}\log\tau}{\mathrm{d}\log\lambda} = 4 - \frac{\mathrm{d}\log Q}{\mathrm{d}\log\lambda} - \frac{\mathrm{d}\log B}{\mathrm{d}\log\lambda} = 4-\beta-\gamma \quad (13)$$

where

$$B = \frac{n^3(m+1)^2(m-1)}{(m^2+2)^2}\frac{\mathrm{d}n}{\mathrm{d}c}; \qquad \beta = \frac{\mathrm{d}\log Q}{\mathrm{d}\log\lambda} \quad \text{and} \quad \gamma = \frac{\mathrm{d}\log B}{\mathrm{d}\log\lambda}$$

For a given wavelength, β depends only on the dimension (D) of the scattering particle. It has been computed by Doty and Steiner [25] for rods and spheres of size range $0 < nD/\lambda < 0.8$. We have computed β and τ for shells of various thickness and the onion-shaped structure. The limiting cases for large D are for a sphere $\beta = 2$, for a long rod $\beta = 1$ and for a thin spherical shell $\beta = 1.83$ [9]. So far the theory is only valid for monodisperse systems, and is adequate for most purposes if the size distribution of particles is sufficiently narrow. We now turn to the problem when the particles are no longer of nearly the same size.

$\star$ To see that Eqn. 8 reduces to the proper expression for a sphere we take the limit of many thin lipid shells with no water. Thus $x_J = jl$, $V = 4\pi/3\ R^3$ and Eqn. 9 reduces to

$$P(\theta) = \left[\frac{3}{Z^3}(\sin Z - Z\cos Z)\right]^2$$

as first stated by Rayleigh [2].

Let the weight concentration of lipid particles be c_j for a given dimensionless size parameter $x_j = nR_j/\lambda$, where R_j is the particle radius. If c is the lipid concentration in the dispersion, then $f_j = c_j/c$ is the weight fraction of particles of size x_j. Using the identity

$$\frac{\mathrm{d}\log\sum f_j(x)}{\mathrm{d}\log x} = \frac{1}{\sum f_j(x)}\sum\left(f_j(x)\frac{\mathrm{d}\log f_j(x)}{\mathrm{d}\log x}\right)$$

It is easily shown that

$$\frac{I(\theta)}{c} = \sum_j f_j I_j(\theta); \qquad \frac{\tau}{c} = \sum_j f_j \tau_j;$$

$$-\frac{\mathrm{d}\log\tau}{\mathrm{d}\log\lambda} = 4-\gamma-\sum_j \frac{f_j\tau_j\beta_j}{\tau/c} = 4-\gamma-\beta_s \tag{14}$$

where $I(\theta)$ is the scattered light intensity and τ the turbidity of the whole dispersion. I_j the specific intensity and τ_j the specific turbidity are the contributions from the j^{th} fraction in the dispersion.

Naturally occurring populations are frequently skewed. We shall assume on the basis of the electron micrograph observations [15, 20] that the distribution of lipid particles behaves similarly. A satisfactory choice of a skewed distribution function is the log-normal distribution [8].

$$f(x) = \frac{1}{\sqrt{2\pi}x\sigma}\exp\left[\frac{-[\ln(x/x_m)]^2}{2\sigma^2}\right] \tag{15}$$

In this distribution, it is ln x rather than x which is normally distributed. The mean value of ln x is ln x_m, σ is the standard deviation, and x_m is the geometric mean of x. Some log-normal distribution curves are shown in Fig. A4. The summations of Eqn. 14 are then replaced by integration.

COMPUTATIONS AND DATA

(a) *Refractive index of lecithin dispersions*

As seen from Eqns. 10–13 the relative refractive index m and the refractive index increment $\mathrm{d}n/\mathrm{d}c$ have to be known for calculations of other quantities. Yi and MacDonald [26] measured these parameters for dipalmitoyl-α-phosphatidylcholine at 589 nm. We have extended the measurements to other wavelengths.

As observed previously [26], the refractive index of the dispersion is a linear function of concentration.

$$n = n_\omega + W\frac{\mathrm{d}n}{\mathrm{d}W} \tag{16}$$

where n_ω is the refractive index of water, W is the weight fraction of lipid and $\mathrm{d}n/\mathrm{d}W$ is the refractive index increment with respect to changes in the weight fraction and is given by the slopes in Fig. 3. n_ω values at different wavelengths, given by the intercepts at the ordinate axis in Fig. 3 agree closely with those reported elsewhere [27].

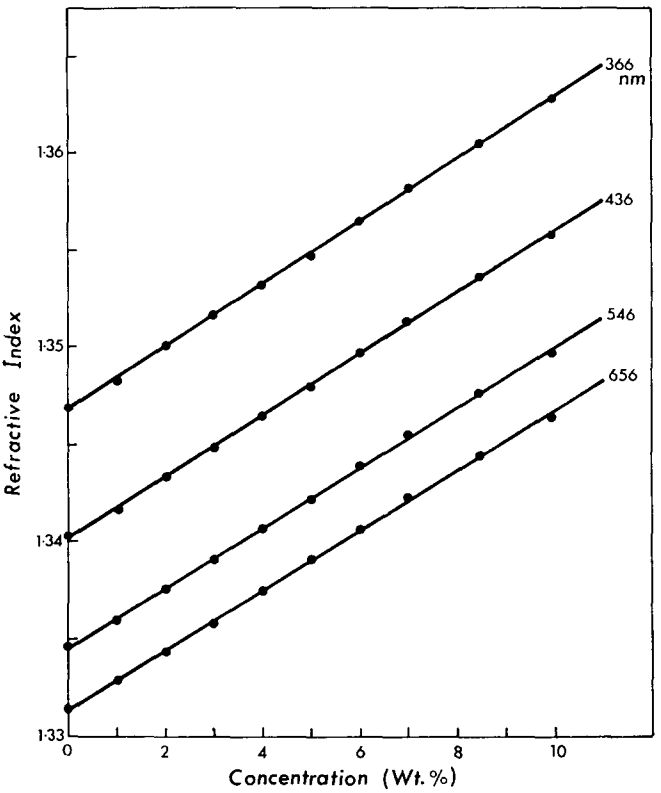

Fig. 3 Refractive index of lipid dispersion as a function of concentration at different wavelengths.

The concentration c(g/ml) is related to the weight fraction W and the density of the dispersion ρ by $c = \rho W$. The density of lecithin $\rho_1 = 1.056$ [23] and thus ρ the density of the dispersion differs only slightly from unity for the range of lipid concentrations used. We can write to a good approximation

$$\frac{dn}{dW} = \rho \frac{dn}{dc} \tag{17}$$

The numerical value of dn/dc is only slightly less than that of dn/dW. Eqn. 15 can now be written in the form

$$n = n_\omega + c \frac{dn}{dc} \tag{18}$$

For 100 % lecithin (i.e. $W \to 1$, $n \to n_1$, $\rho \to \rho_1$) we obtain

$$n_1 = n_\omega + \rho_1 \frac{dn}{dc} \tag{19}$$

Knowing n_1 and n_ω we can calculate the relative refractive index m, the parameter B, and the factor γ (Eqn. 13) for different wavelengths (Fig. 4). The results of the calculations are given in Table I.

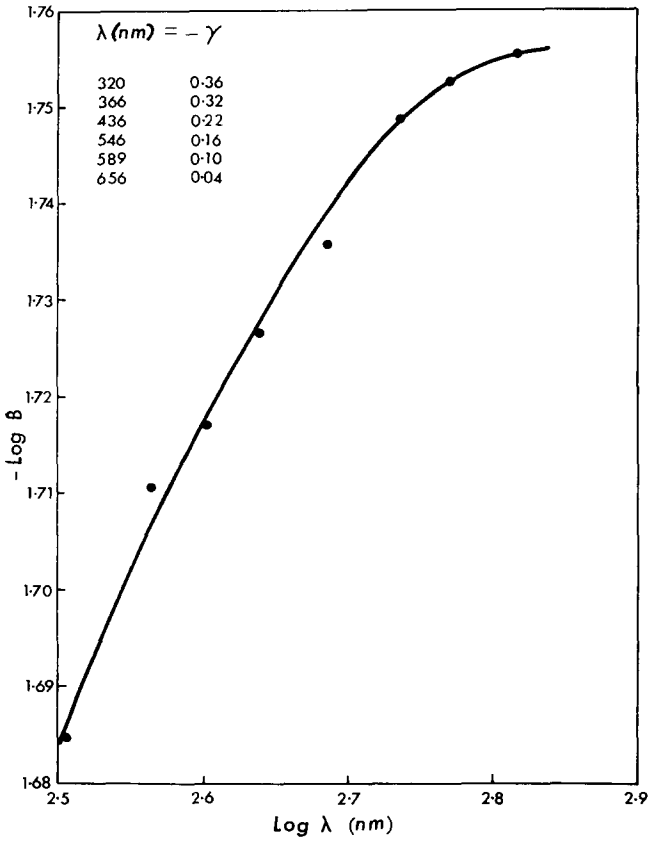

Fig. 4. Log-log plot of B (Eqn. 13) as a function of wavelength. The power γ is obtained from the tangent to the curve.

The temperature dependence of the refractive index of a 10 % lipid dispersion is shown in Fig. 5 along with that of water. The difference between the two curves gives the change of the lipid alone, which shows a significant drop in the refractive index at about 41 °C as observed previously [26]. We can now evaluate the changes of dn/dc and m at the phase transition and hence calculate the changes in scattered light intensity and turbidity.

Although the refractive index changes were measured at 589 nm, we can assume proportionate changes at other wavelengths. We obtained the following values at 45 °C for the wavelength of 436 nm: $n_1 = 1.460$, $n_\omega = 1.329$, $dn/dc = 0.132$, $m = 1.100$.

(b) *Monodisperse systems*

We have computed the quantities $I(90\ °C)/c$, β and τ/c for both models shown in Fig. 1. Computer plots are given in Appendix.

The single shell model is not a good model for normally prepared lipid dispersions. The usefulness of the calculations is limited to small values of the size parameter. It is of interest to note from Figs. A1 and A2 that the β values calculated

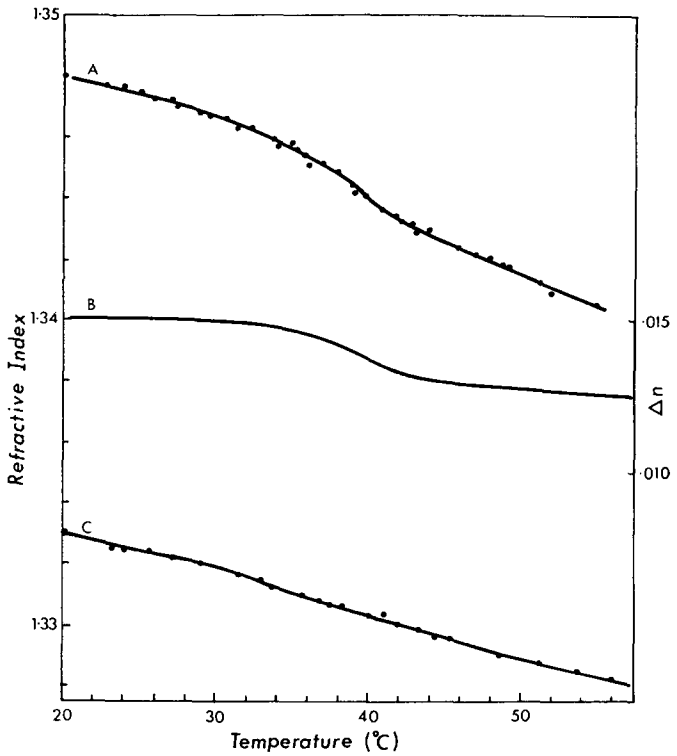

Fig. 5. Temperature dependence of the refractive index of a 10 % lipid dispersion. Curve A applies to the lipid dispersion, C to water, and B is the difference between A and C (right scale).

TABLE I

REFRACTIVE INDEX OF LECITHIN DISPERSIONS AT 20 °C AND DIFFERENT WAVELENGTHS

γ is obtained from a plot of log B versus log λ (Eqn. 13) using refractive indices of water and lipid dispersions of different concentrations.

Wavelength (nm)	n_ω	n_1	dn/dc	m	$-\gamma$
366	1.347	1.507	0.160	1.120	0.32
436	1.340	1.497	0.157	1.117	0.22
546	1.334	1.488	0.154	1.115	0.16
589	1.333	1.486	0.153	1.115	0.10

for both models are not much different when the particles are sufficiently large and have the same water core radius and the same size. However, from Figs. A1 and A2, the turbidity for the second model is about 0.6 of that of the first model. In view of the actual multi-lamellar structure, one should have used an effective relative refractive index in the calculation of turbidity for model 1. From Eqn. 12, one finds that a change in the relative refractive index changes the turbidity mainly through the term $(m-1)$. A choice of $m' = 1.07$ for the effective relative refractive index would give the ratio of 0.6 for the turbidities.

We shall now describe the procedure for estimation of size and structure of lipid particles in a monodisperse system. The turbidity of the dispersion is first obtained for a range of wavelengths (300–650 nm) using a conventional spectrophotometer, and is displayed on a log-log plot. The gradient of the curve say at 436 nm is found and β can then be calculated from Eqn. 13, knowing the value of γ. The specific turbidity τ/c at 436 nm can also be calculated knowing both the turbidity τ and the concentration of lipid in the dispersion. Fig. A2 or A1 is then examined. The size parameter which gives the best match of the measured values of both β and τ/c to the calculated values provides a reasonable estimate of the mean size and structure of the lipid particles in the dispersion. If a good match for both β and τ/c cannot be found, the particles are assumed to have a wide range of sizes and the calculations for polydisperse systems have to be used. Generally, it was found that if the measured absorbance was less than 0.10 for a concentration of 1 mg/ml, the distribution was sufficiently narrow and the average radius of the particles less than 400 Å.

(c) *Polydisperse systems*

The quantities $I(90°)/c$, τ/c and β_s were calculated using Eqn. 14 for a variety of log-normal distributions. We shall call these values the effective scattering, effective

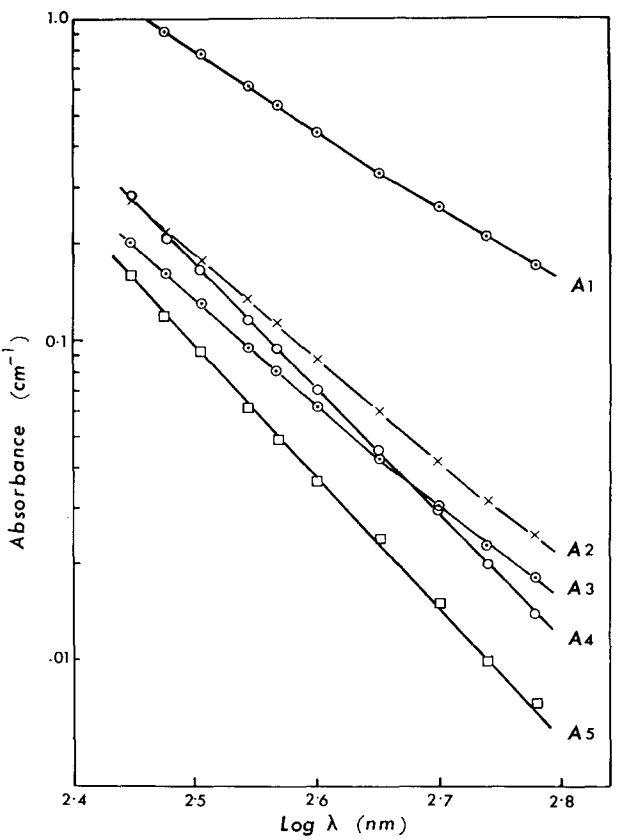

Fig. 6. See opposite page for legend.

TABLE II

SOME LIPID DISPERSIONS AND THE EXPERIMENTAL VALUES OF THE POWER FACTOR β, AND THE SPECIFIC TURBIDITY τ/c AND SCATTERING $I(90°)/c$ AT THE WAVELENGTH OF 436nm

Log-log plots of the absorbances against wavelength for these dispersions are shown in Fig. 5.

Sample	Treatment*	Concentration (mg/ml)	β	τ/c	$I(90°)/c$ relative units
A1	10 min, no filtration	0.76	1.70	1.05	214
A2	from A1, ultracentrifuge	0.54	1.03	0.29	87
A3	from A1, 0.45 μm filter	0.46	1.02	0.23	102
A4	from A3, 0.2 μm filter	0.39	0.32	0.28	66
A5	40 min, 0.2 μm filter	0.36	0.16	0.16	30
B1	3 min, no filtration	0.43	2.40	4.40	837
B2	from B1, 1.0 μm filter	0.14	1.90	1.35	272
B3	from B2, 0.2 μm filter	0.070	1.35	1.25	270
B4	from B1, ultracentrifuge	0.050	1.80	2.14	480
C	5 min, no filtration	0.90	1.50	0.87	192
D	5 min, no filtration	0.76	1.10	0.32	88
E	5 min, no filtration	0.12	1.80	1.41	181

* Time denotes the time of sonication and the size unit is the pore size of the metricel filter.

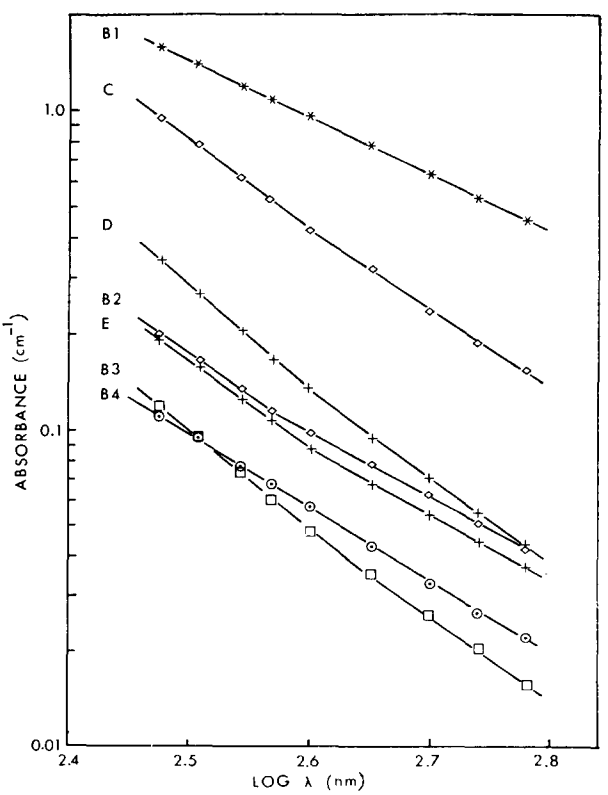

Fig. 6. Log-log plot of absorbance as a function of wavelength for some lipid dispersions. (See Table II for sample labelling).

turbidity and effective power factor, respectively. The $I_j(90°)$, τ_j and β_j values are those already calculated for the monodisperse system. We have only computed the effective values at 436 nm for the multilamellar model with no central water core. The correction taking into account the enclosed volume of water in the aqueous core is minimal. The results of the computations are shown in Fig. A3. To estimate the size distribution of lipid particles in the dispersion, the experimental values of τ/c and β_s were matched against those in Fig. A3, which was always possible. A few examples are given below, using the lipid dispersions listed in Table II.

(d) *Size estimation for some lipid dispersions (Table II)*

Sample A1. From Fig. 2A for the multilamellar model, one finds for $\beta = 1.70$, $x = nR/\lambda \simeq 0.52$ for all six aqueous core radii. Thus the outer radius R $\simeq$ 1600 Å for $\lambda = 436$ nm and $n = 1.340$. However, $\tau/c = 1.05$ is rather low for a monodisperse system. It is not possible to match the measured β and τ/c to the computed values for the same size parameter x. From Figs. A1 for the single shell model one finds that for $x \simeq 0.46$, $\beta \approx 1.7$ and $\tau/c \approx 1.8$ for the ratio of inner/outer radius $t = 0.9$. Multiplying τ/c by 0.6 to take into account the multilamellar structure, we obtain the corrected value of 1.08 for the computed τ/c. Thus the size parameter $x = 0.46$ and the ratio $t = 0.9$ provide a reasonably good match of the experimental values of β and τ/c to the computed values. The average size and structure of the lipid particles can now be estimated from the value of the size parameter x and the ratio t. We find that the mean radius is about 1500 Å and the thickness of the lipid-water shell is about 135 Å. On examination of the concentrations of the samples A2, A3 and A4 which were derived from A1, one can deduce that 1/3–1/2 of the concentration of lipid in A1 is in the form of vesicles of this size.

Using Fig. A1 and the corrected τ/c values for matching, one finds the lipid particles in samples B2, B4 and E have a mean radius of about 2000 Å. In general, dispersions which exhibit high β (about 1.8) and τ/c of about 1–2, contain a rather wide distribution of lipid particles with large aqueous cores.

Samples A2, A3, and D. From Fig. A1, for $x = 0.16$ and $t = 0.9$ one finds $\beta = 1.1$ and $\tau/c = 0.36$. Correcting for the multilamellar structure gives $\tau/c \approx 0.24$. Thus for samples A2, A3 and D, the average radius is about 550 Å with a bilayer thickness of about 50 Å. Examination of Fig. A2 gives the same estimate.

Sample A4. For this sample a mean radius of 300 Å was estimated. Two alternative multilamellar structures would provide the right β and τ/c values: (a) Four concentric lipid layers and no aqueous core, (b) two or three concentric layers with an aqueous core of 100–200 Å.

The possible presence of rod-like particles was also investigated since these give rise to β values of less than one over a wide range of length of the particle [26]. From the tables calculated by Doty and Steiner [26], $\beta \approx 0.32$ is obtained for a rod of about 1000 Å length. To satisfy $\tau/c = 0.28$, the rod has to be about 160 Å in radius which is much larger than the 20 Å for the rod-like micelles observed by Bangham and Horne [18]. The presence of such a large rod-like particle was further discounted on the basis of the very small depolarisation ratio in the light scattering although the smaller rod-like micelles could be present in small quantities.

There seems to be an apparent discrepancy when one considers samples A3 and A4 together. A4 was derived by passing A3 through a 0.2 μm filter. As only about

15 % of the weight of A3 was filtered out, one would expect A4 to show the characteristics of A3 since the pore size of 0.2 μm was larger than the mean diameter of the vesicles in A3. A possible explanation is that the larger vesicles somehow collapsed during the filtration process to give smaller vesicles with more concentric bilayers.

Sample A5. The most probable structure is that of a single bilayer vesicle of radius 200 Å.

Sample B1. The abnormally high value of $\beta(> 2)$ implies the presence of a large percentage of large particles. In this case, the Rayleigh-Gans approximation is not valid. However, the value of τ/c which is not too high also implies that a substantial amount of the particles had a radius of about 2000 Å. This conclusion is supported by the data of the sample B2 which was obtained by filtering B1 with a 1 μm pore metricel filter.

Sample B3. It is quite hard to find matching values from Fig. A1 or Fig. A2; we thus turn to Fig. A3. A log-normal distribution of geometric mean $x_m = 0.12$ and a standard deviation $\sigma = 0.8$ would give the right β and τ/c.

Sample C. From Fig. A2 we find that a size parameter $x \simeq 0.22$ and an inner core radius of 500 Å would provide the match for the β and τ/c values. This means the average particle had an outer radius of 700 Å and two or three concentric lecithin bilayers.

The specific 90° scattered light intensity was not used to provide estimation of the particle sizes since (1) the scattered light intensity was not an absolute measurement, (2) its oscillatory nature as a function of size parameter limits its usefulness, and (3) the range of validity of the Rayleigh-Gans approximation is smaller. It was shown for solid spheres [8] that τ/c agreed with the more rigorous Mie theory to within 10 % for values of $nR/\lambda \lesssim 1.5$, whereas the range of validity for the scattered light intensity decreased rapidly for increasing angle of scattering. The same conclusion should hold for the multilamellar structure. Nevertheless, the observed relative scattered light intensity (Table II), particularly for smaller lipid particles, followed the computed values. 90° scattered light intensity measurements are useful when the size distribution is sufficiently narrow and the size parameter is less than 0.2.

The oscillatory region of the scattering factor $P(\theta)$ can be avoided by going to low angle scattering. One may determine particle sizes from a Zimm plot [8, 28] by utilising the angular variation of scattering close to the forward direction. The Zimm plot method provides a distinct advantage over the turbidity method of size estimation since it leads to a measure of both the molecular weight and the radius of gyration, independent of any assumptions regarding the shape of the particle. However, instrumental calibration and precise measurements of angles are necessary to obtain good results.

So far, we always considered our vesicles to be spherically symmetric. Nonspherical particles give rise to a depolarisation ratio $\rho = H/V$ of scattered light intensities polarised horizontally (H) and vertically (V) to the plane of incidence, for vertically polarised incident light. The turbidity is then modified for small particles by the correction factor [8] $C = (3+6\rho)/(3-4\rho)$. For the dispersions prepared, $\rho \approx 0.03$, which amounts to a correction of less than 6 %, if we ignore the size factor of the vesicles, which limits the validity of the above correction factor. It was observed that ρ was always smaller above the transition temperature, which implies an increase in spherical symmetry at higher temperatures.

TEMPERATURE DEPENDENCE OF SCATTERED LIGHT INTENSITY AND TURBIDITY

The dispersions listed in Table II were studied at different temperatures. Fig. 7 shows the temperature dependence of the scattered light intensity and turbidity of two samples. In Fig. 8 the turbidity of these samples as a function of wavelength at temperatures below and above the phase transition are shown. Sample B1 showed a large drop in both the scattered light intensity and turbidity just before the phase transition temperature during the first heating cycle. Subsequent cooling and re-heating did not show this anomalous change. The second heating/cooling cycle revealed almost identical temperature dependence as that in the first cooling cycle. Sample D did not exhibit such an anomalous change. Second heating/cooling curves were identical to those of the first cycle. Samples B3 and A4 showed similar behaviour than B1 and D, respectively [22].

We shall now consider the effects of changes of the refractive index increment dn/dc, relative refractive index m and the volume V on the post-transition scattering and turbidity. In Fig. 5, dn/dc was shown to decrease by about 16 % from 20 to 50 °C. A change in m leads to an additional change in the turbidity and scattered light intensity (Eqns. 11 and 12), primarily through the change in the term $(m-1)$. This gives a further decrease of about 15 %. As observed by Sheetz and Chan [20], the

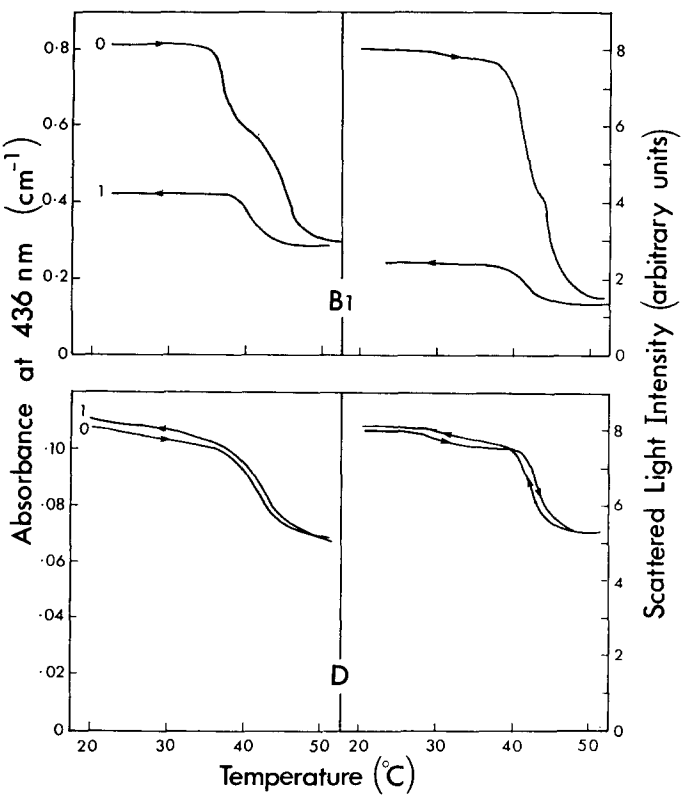

Fig. 7. Temperature dependence of scattered light intensity and absorbance of two lipid dispersions.

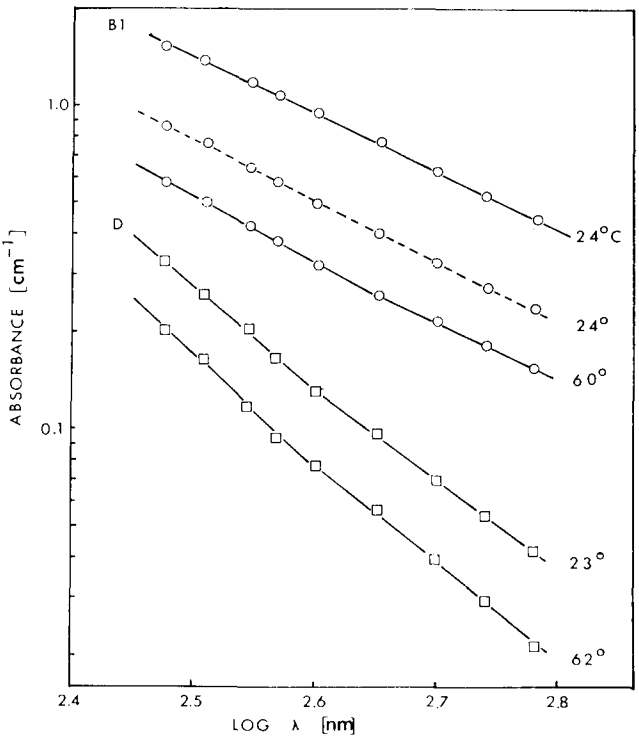

Fig. 8. Change of absorbance with temperature for two lipid dispersions. The dotted line is for the observation on the cooling cycle. The cooling cycle observation for sample D at 24 °C is about the same as that for 23 °C and is thus not shown.

lipid volume in the vesicles increased by about 3 %. Assuming that during the phase transition the lipid layer thickness decreased from 45 to 40 Å [30] while the water layer thickness increased from 25 to 30 Å so as to maintain the shape of the vesicles, we find that comparing the appropriate calculations [22] that there would be an additional average decrease of about 7 % in the turbidity or scattered light intensity. In all, there should thus be an overall drop of about 32 % (i.e. obtained from $1-0.84\times 0.85\times 1.03\times 0.93$) in the scattered light intensity or turbidity between 20 and 50 °C. This change was observed in samples D and A4 during all the heating/cooling cycles and in samples B1 and B3 only during the first cooling cycles and subsequent heating/cooling cycles. We shall have to look for other effects that could cause the irreversible anomalous change in samples B1 and B3 during the first heating cycle.

At first thought, precipitation of large lipid aggregates could have caused the anomalous change. However, examination with a light microscope did not reveal large lipid particles in these samples. Furthermore, in some mildly sonicated samples in which precipitation did take place, the scattered light intensity and turbidity during temperature runs showed large fluctuations as the large aggregates crossed the path of the incident beam. We propose that before heating in the first cycle, a large percentage of scattering particles in samples B1 and B3 was in the form of aggregates of smaller vesicles. These aggregates (Fig. 9) from light scattering or turbidity measurements

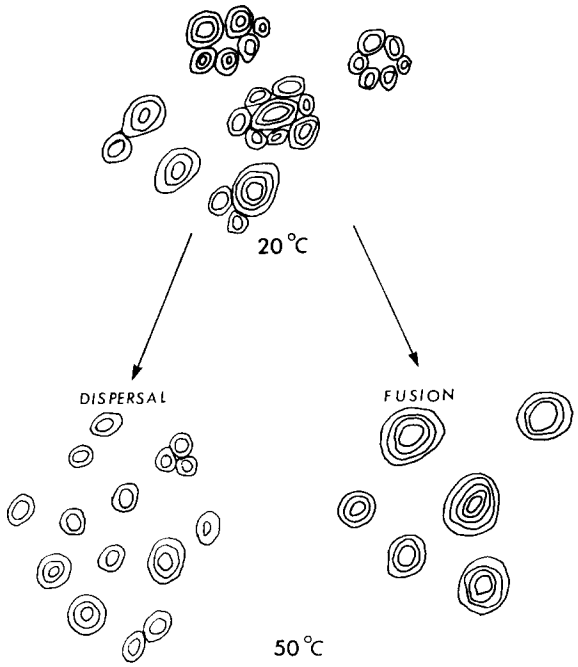

Fig. 9. Dispersal and fusion of lipid vesicle aggregates.

would be detected as though they were large multilamellar vesicles. As confirmed by the measured higher depolarisation ratio they were less spherically symmetric. The scattering, turbidity and β value of a dispersion with such aggregates would be higher than a corresponding dispersion of the same concentration with no aggregation effects. Near the phase transition temperature, two processes could be facilitated: (1) The breaking up of aggregates into the smaller component vesicles, leading to reduced scattering and turbidity, and a smaller β. (2) Fusion of vesicles in the aggregate forming smaller multilamellar vesicles with aqueous cores and leading to reduced turbidity and scattering. The β value would generally remain the same or increase slightly. One or both of these processes could occur. In view of the slight increase of β at the post-transition temperature the fusion process should be predominant for dispersions B_1 and B_3. This would also account for the dissimilar first heating and cooling curves as the fusion process is not reversible.

DISCUSSION

The power factor and the specific turbidity computed on the basis of Rayleigh-Gans theory provide a rapid means of estimating the size and structure of lipid particles in a dispersion from turbidity measurements. Values computed for the multilamellar model are useful for reasonably sonicated dispersions which show a β value of less than 1.5. For larger particles with probably large inner aqueous cores, one has to resort to the values computed for the single lipid shell model. In view of the multilamellar structure not taken into account in this model, the relative refractive index has to be replaced by an effective value.

An attempt was made to include the effect of polydispersity by calculating the effective power factor and turbidity. Log-normal distributions were assumed and only the multilamellar model with no aqueous core was taken into account. Calculations for the multilamellar model with different inner core radii would extend the applicability.

In matching experimental values of β and τ/c to the calculated values, the lipid bilayer thickness $l = 45$ Å and water layer thickness $\omega = 25$ Å were used. Computations for other values of l and ω may be used to see if a closer match can be obtained. Also matching at another wavelength is desirable to check the consistency of the size estimate.

Our estimates of liposome sizes and structures in some sample dispersions support the observation that prolonged sonication produces small single bilayer vesicles. For dispersions which have undergone short periods of sonication, the scattering and turbidity are due predominantly to large vesicles with large aqueous cores, some of which may be aggregates of smaller vesicles. These large vesicles constitute about one-third of the lipid concentration and may be removed by filtration or ultracentrifugation.

From the temperature dependence of the refractive index of lipid dispersions we have shown that the normal reversible decrease of about 32 % in scattered light intensity or turbidity between 20 and 50 °C could for a large part ($\approx 7/8$) be accounted for by the decrease in the refractive index of the lipid at the phase transition. The change in volume and bilayer thickness of the vesicles at the phase transition could account for the remaining change in scattering.

Aggregation and fusion processes could account for the irreversible anomalous changes in the scattered light intensity and turbidity of some dispersions near the phase transition temperature. Fusion of small vesicles in the aggregates could result in a large drop in scattered light intensity and turbidity of a dispersion. Preliminary work showed that the addition of Ca^{2+} to the lipid dispersion and a change in pH caused dramatic changes in the temperature dependence of light scattering. Light scattering and turbidity measurements should provide a useful tool in studying the effects of ions on the size, structure, aggregation and fusion processes of lipid vesicles and such studies would provide a better understanding of membrane fusion.

APPENDIX

Computer calculations of the scattering parameters at a wavelength of 436 nm for the single shell and the multilamellar model of vesicles

For the single shell model six ratios (t) of inner aqueous core radius to outer radius of the vesicle were considered, up to a maximum vesicle size about equal to the incident wavelength of light. $P(\theta)$ was first calculated using Eqn. 7, for various values of kR. $I(90°)/c$, Q, β and τ/c were then obtained for various values of the size parameter, nR/λ.

For the multilamellar model six aqueous core radii and 50 concentric lipid bilayers were considered. The choice of lipid layer thickness $l = 45$ Å and water layer thickness $\omega = 25$ Å was based on electron micrograph observations and X-ray diffraction [18, 29]. $I(90°)/c$ and τ/c are specific values normalized for a lipid concentration of 0.1 and 1 mg/ml, respectively.

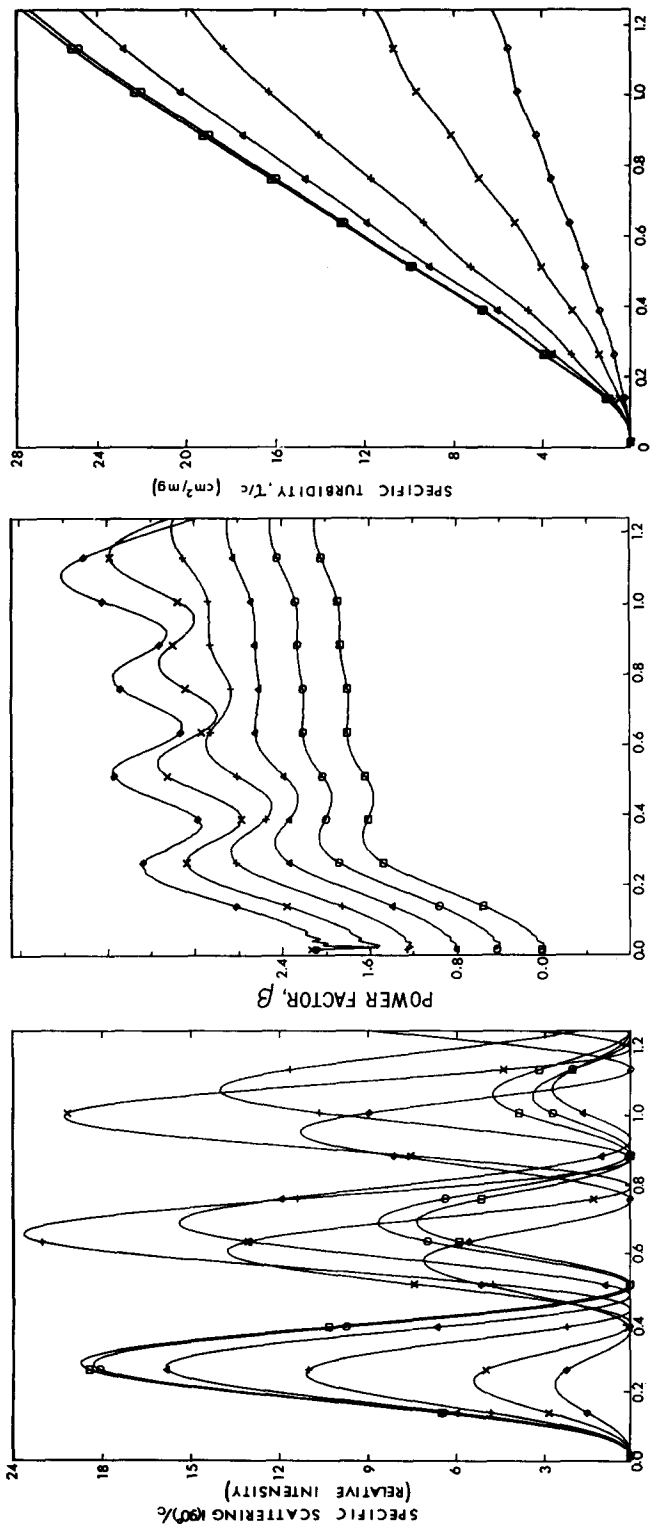

Fig. A1. Specific scattering, specific turbidity, and power factor as a function of size parameter for single lipid shell vesicles of various ratios of inner to outer radius (□ =0, ○ = 0.2, △ = 0.4, + = 0.6, × = 0.8, and ◇ = 0.9).

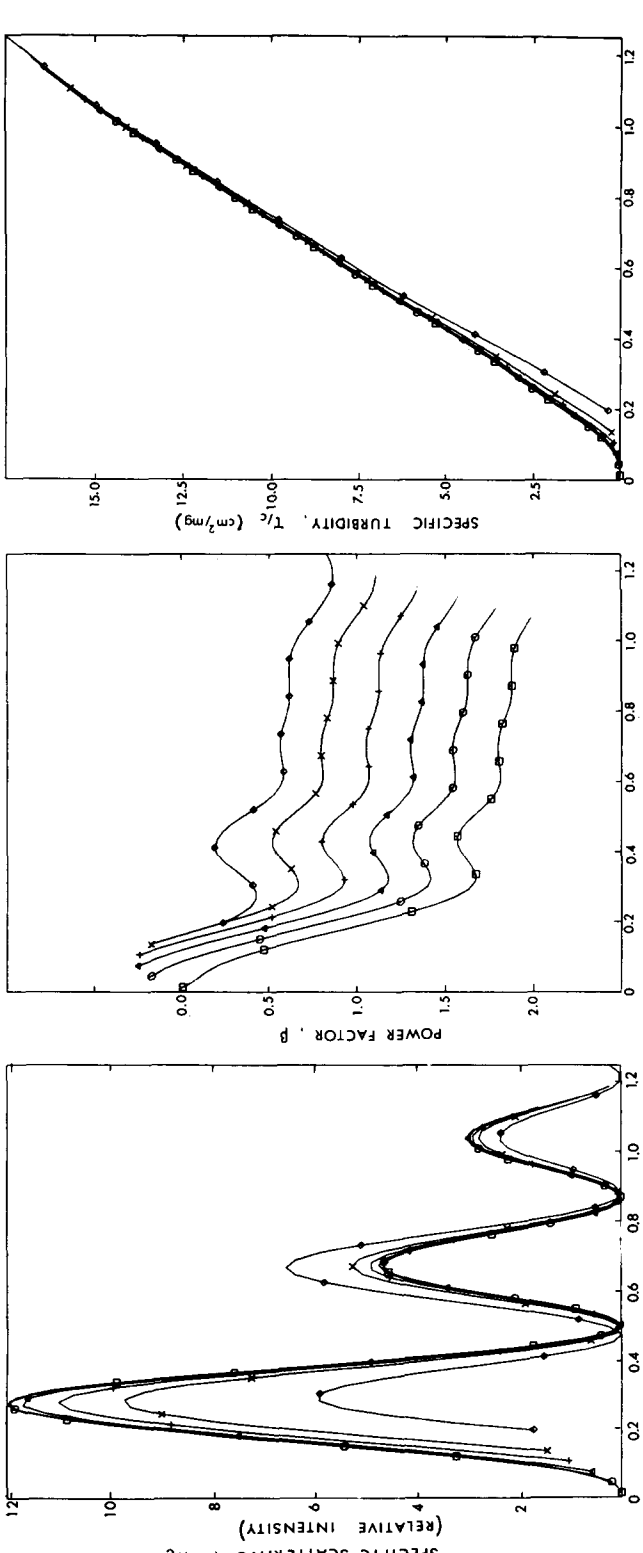

Fig. A2. Specific scattering, specific turbidity, and power factor a as function of size parameter for multilamellar vesicles of different aqueous core radii ($\square = 0$, $\bigcirc = 100$, $\triangle = 200$, $+ = 300$, $\times = 400$, and $\diamond = 600$ Å).

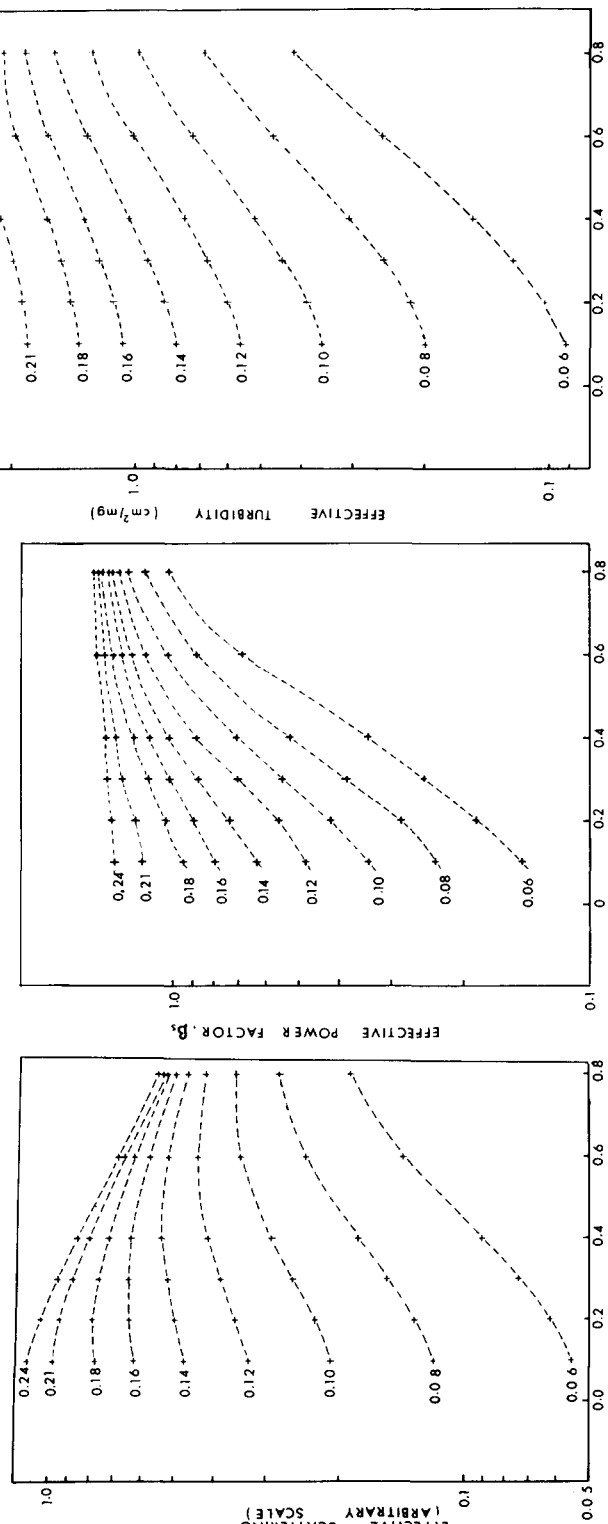

Fig. A3. Variation of effective scattering, effective power factor, and effective turbidity for different log-normal distributions. The numbers beside the curves denote the geometric mean x_m of the size distributions.

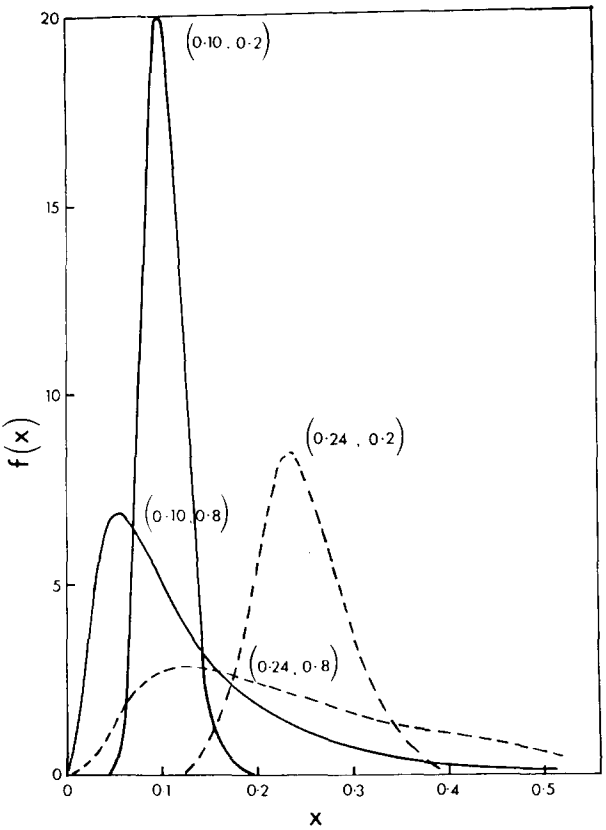

Fig. A4. Some log-normal distribution curves. Each pair of numbers denotes the geometric mean x_m and the standard deviation σ of the distribution.

For the power factor in Figs. A1 and A2, the origins of the curves for different core radii are displaced with respect to each other. Fig. A3 shows the scattering parameters for polydispersed systems with various log-normal distributions and no central water core. Examples of some log-normal distributions are given in Fig. A4.

More extensive tables and figures covering different scattering wavelengths, as well as the computer programs, are available on request.

ACKNOWLEDGEMENT

This work was supported by the National Research Council of Canada.

REFERENCES

1 Rayleigh, Lord (1881) Phil. Mag. 12, 81–101
2 Rayleigh, Lord (1914) Proc. R. Soc. Lond. Ser. A, 90, 219–225
3 Debye, P. (1915) Ann. Physik 46, 809–823
4 Gans, R. (1925) Ann. Physik 76, 29–38
5 Mie, G. (1908) Ann. Physik 25, 377–445
6 Debye, P. (1909) Ann. Physik 30, 57–136

7 Van de Hulst, H. C. (1957) Light Scattering by Small Particles, John Wiley and Sons, London
8 Kerker, M. (1969) The Scattering of Light, Academic Press, New York
9 Koch, A. L. (1961) Biochim. Biophys. Acta 51, 429–441
10 Wallach, D. F. H., Kamat, V. B. and Gail, M. H. (1966) J. Cell Biol. 30, 601–621
11 Atwood, D. and Saunders, L. (1965) Biochim. Biophys. Acta 98, 344–350
12 Abramson, M. B. (1971) Biochim. Biophys. Acta 225, 167–170
13 Overath, P. and Träuble, H. (1973) Biochemistry 12, 2625
14 Sackman, E. and Träuble H. (1972) J. Am. Chem. Soc. 94, 4482–4491
15 Seufert, W. D. (1970) Biophysik 7, 60–73
16 Tinker, D. O. (1972) Chem. Phys. Lipids 8, 230–257
17 Huang, C. (1969) Biochemistry 8, 344–352
18 Bangham, A. D. and Horne, R. W. (1964) J. Mol. Biol. 8, 660–668
19 Chapman, D., Fluck, D. J., Penkett, S. A. and Shipley, G. G. (1968) Biochim. Biophys. Acta 163, 255–261
20 Sheetz, M. P. and Chan, S. I. (1972) Biochemistry 11, 4573–4581
21 Chan, S. I., Sheetz, M. P., Seiter, C. H. A., Feigensen, G. W., Hsu, M. C., Lau, A. and Yau, A. (1973) Ann. N.Y. Acad. Sci. 222, 499–522
22 Chong, C. S. (1975) Simon Fraser University, Ph. D. Thesis
23 Raheja, R. K., Kaur, C., Singh, A. and Bhatia, I. S. (1973) J. Lipid Res. 14, 695–697
24 Oster, G. and Riley, D. P. (1952) Acta Cryst. 5, 1–6
25 Doty, P. and Steiner, R. F. (1950) J. Chem. Phys. 18, 1211–1220
26 Yi, P. N. and MacDonald, R. C. (1973) Chem. Phys. Lipids 11, 114–134
27 American Institute of Physics Handbook (1957) pp. 5–140, McGraw-Hill Book Co., New York
28 Zimm, B. H. (1948) J. Chem. Phys. 16, 1099–1116
29 Chapman, D., Williams, R. M. and Ladbrooke, B. D. (1967) Chem. Phys. Lipids 1, 445–475